applied sciences

MDPI

Article

Optimal Energy Management Systems and Voltage Stabilization of Renewable Energy Networks

Mohamed-Dhiaeddine Drid [1], Samir Hamdani [1], Amirouche Nait-Seghir [1], Larbi Chrifi-Alaoui [2], Sami Labdai [2] and Said Drid [3,*]

[1] Electrical and Industrial Systems Laboratory, University of Science and Technology Houari Boumediene, Bab Ezzouar, Algiers 16111, Algeria; mdrid1@usthb.dz (M.-D.D.); shamdani@usthb.dz (S.H.); amirouche.nait-seghir@usthb.edu.dz (A.N.-S.)
[2] LTI (UR-UPJV-3899), University of Picardie Jules Verne, 80000 Amiens, France; larbi.alaoui@u-picardie.fr (L.C.-A.); sami.labdai@u-picardie.fr (S.L.)
[3] Laboratory LEREESI, Higher National School of Renewable Energy, Environment and Sustainable Development, Constantine Road, Fesdis, Batna 05078, Algeria
* Correspondence: s.drid@hns-re2sd.dz or s_drid@yahoo.fr

Abstract: This paper addresses the challenge of integrating multiple energy sources into a single-domain microgrid, commonly found in urban buildings, while also providing a platform for energy management. A Lyapunov stability analysis of a simple boost converter was used as a basis for designing the dual control loop of the grid. The versatility of the developed control structure allows for the incorporation of an arbitrary number of sources hence achieving scalability. Next, the energy in the microgrid was separated into exogenous energy and actuator energy. This yielded a description of the system that quantified the condition of stability independent of the decision made by a would-be energy management system. This, in turns, liberates the process of designing an optimized energy management system from stability concerns. The acquired theoretical findings were then translated to a simulation model, where multiple components of the grid were simulated under a typical scenario of operation. Once the simulation phase was concluded, a prototype of the designed grid was constructed to emulate the theoretical results. The prototype exhibited promising performance, matching the simulation predictions to a reasonable degree.

Keywords: microgrids; energy management; multi-source; building; urban; optimized energy management; scalability

check for updates

Citation: Drid, M.-D.; Hamdani, S.; Nait-Seghir, A.; Chrifi-Alaoui, L.; Labdai, S.; Drid, S. Optimal Energy Management Systems and Voltage Stabilization of Renewable Energy Networks. *Appl. Sci.* **2024**, *14*, 9782. https://doi.org/10.3390/app14219782

Academic Editors: Levon Gevorkov and Olena Rubanenko

Received: 27 August 2024
Revised: 2 October 2024
Accepted: 3 October 2024
Published: 25 October 2024

Copyright: © 2024 by the authors. Licensee MDPI, Basel, Switzerland. This article is an open access article distributed under the terms and conditions of the Creative Commons Attribution (CC BY) license (https://creativecommons.org/licenses/by/4.0/).

1. Introduction

Microgrid (MG) technology was reintroduced as a transient solution for current sustainability challenges in the energy sector. Until cleaner and more powerful methods of producing and transporting electricity are found; the best course of action would be to aim for an increase in efficiency. By miniaturizing and distributing the power production across the network, the distance between the energy source and the load is reduced, this leads to less transportation losses. Additionally, integrating clean resources such as solar and wind driven power plants, will subsequently alleviate the burden of power generation on the utility grid. These systems, known as multi-source microgrids, exhibit inherent fault tolerance under appropriate conditions, attributable to the diversity of their power inputs. Depending on the penetration of renewables in a microgrid, off grid or islanded mode may be attained, this is especially advantageous in remote areas or in difficult terrain where establishing a conventional grid is not economically viable [1–3].

Although the term microgrid is ubiquitously used in academia there is no universal definition that contains it. The U.S. Department of Energy (DOE) defines a microgrid as "a group of interconnected loads and distributed energy resources within clearly defined electrical boundaries that acts as a single controllable entity with respect to the grid. A

microgrid can connect and disconnect from the grid to enable it to operate in both grid-connected or island-mode" [4]. On the other hand, the Consortium for Electric Reliability Technology Solutions (CERTS) defines a MG to be "a better way to realize the emerging potential of distributed generation in a systematic approach which views generation and associated loads as a subsystem" [5].

A MG clearly has the potential to be a platform for achieving sustainability reliability and profitability, however it does not guarantee it. To achieve these objectives, it is essential to implement an energy management system. This can be accomplished through the utilization of electrical storage systems or by incentivizing end-users to engage in load shifting or load shedding. The system's performance must comply with specific quality control standards, which primarily translates to a stability issue. In other words, the system must maintain a consistent quality despite any perturbations.

A substantial body of literature, as referenced in sources [6–12], enumerates and catalogs MG topologies and structures observed in real-world applications. This literature also details the technologies employed for stabilizing the voltage bus and the methodologies for implementing energy management systems under various economic criteria for both AC and DC microgrids. One trend that can be observed is proliferation of DC MGs, although the AC counterpart enjoy perks such as an already established mega infrastructure (utility grid) as well as maturely developed protection apparatus. Researchers increasingly favors the use of DC or AC/DC microgrids due to their inherent compatibility with solar panels and batteries, as well as the ease of converting from AC to DC. Furthermore, the rising consumption of DC loads in urban areas, such as electric vehicles and LED lighting, further supports the integration of this technology in urban settings.

A multitude of studies have been conducted to tackle the challenges of integrating renewable energy sources into microgrids. In [13], a distributed supervisory secondary control scheme was developed to address the problem of voltage regulation and current sharing amongst a number of energy sources. This was achieved by switching between two candidate voltage and current controllers. Whereas in [14], an optimally-coordinated and cooperative multi-layered EMS was formulated with a consensus algorithm. This study concentrated more on scalability in real-time, privacy, and improved reliability. A droop-based fully decentralized architecture is proposed in [15], where an adaptive droop control is employed in a multi-source DC grid to manage both voltage and power. The study implemented an algorithm that takes into consideration the energy pricing and the state of charge, without the use of communication lines. In [16], an EMS was implemented in a 1 KW prototyped MG. The primary goal of this study revolved around robustness and optimization of energy production. Another stability-focused study in [17] conducted an observation on the stability of a DC microgrid based on a pre-planned transaction schedule on a university campus in Korea. In [18], A robust current control based on Lyapunov theory was implemented using a multiport converter for hybrid renewable PV-Wind energy systems. The study deployed a dSPACE-DS1104 effectively to implement the proposed control.

All of the aforementioned studies conducted the work on a DC microgrid, either focusing one particular aspect, be it stability related or energy management related but seldom both at in tandem, with bulk of the testbed developed being concerned more with the step response effect on stability. There are few articles that discusses the effect of energy management on the stability of the MG.

The work done in paper is primarily concerned with the design of a stable multi-source microgrid in purview of energy management with the following contributions:

- The generalization of the regulation and the optimization problem in the MG
- Creation and Implementation of a versatile simulated model of a MG
- Real practical application of the model in an experimental testbed

The paper is organized as follows; Section 2 compiles the theoretical notions used for the formulation of the model and control structure, serving as a precursor for energy analysis. Next in Section 3, a graphical interpretation of the consumption profile, projected onto

the optimization objectives, is conducted. This approach provides a clear understanding of the effective strategies employed for subsequent analysis. Section 4 provides a detailed account of the simulation model constructed from the previous finding in Sections 2 and 3, afterwords the results are displayed and interpreted. Section 5 discloses the experimental results obtained and components deployed in light of the theoretical study. Finally, the paper ends with a conclusion that summaries the undertakings of this paper and experimental notes regarding the nuances of the realization process.

2. System Layout

The total flow of energy delivered from any number of sources in a MG to the end user can be modelled as a single current controlled source of a setpoint (I^*_{ref}) connected to a parallel RC branch, through the principle of superposition, a single virtual source can be constructed in Figure 1.

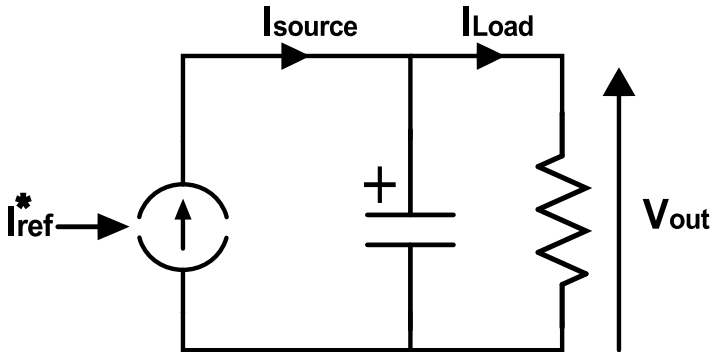


Figure 1. Microgrid single current sources model.

There are two key dynamics of interest within the system. The first is of the output voltage (V_{out}) in response to the input current (I_{source}), as the derivative of the bus voltage is proportional to the imbalance between the supply current and the load current (I_{load}).

$$\frac{dV_{out}}{dt} = \frac{1}{C}(I_{source} - I_{load}) \tag{1}$$

$$I_{load} = \frac{V_{out}}{R_{load}} \tag{2}$$

This subsequently leads to the transfer function relating the output voltage and the input current where R_{bat} is the load's resistance

$$\frac{V_{out}}{I_{source}} = \frac{R_{load}}{(R_{load}C \cdot s + 1)} \tag{3}$$

The second dynamic of interest is that of the input current in response to the input current reference (I_{ref}). There are a multitude of apparatus that can achieve current control mode of an electric source, regardless, as with any real system, it is quite reasonable to assume that such systems are quantifiable, usually using a nonlinear second order system to encapsulate common characteristics such as natural frequency (ω_n), Damping coefficient (ζ), settling time, overshoot, steady-state error, etc.

$$\frac{I_s}{I_s^{ref}} = \frac{\omega_n^2}{s^2 + 2\zeta\omega_n \cdot s + \omega_n^2} \tag{4}$$

To validate this assumption a simple boost converter is deployed as shown in Figure 2.

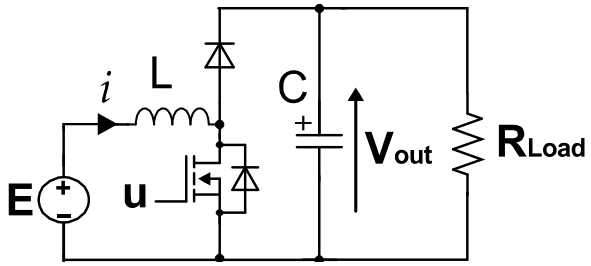


Figure 2. Schematics of the boost converter.

The control signal "u" dictates the conduction state of the MOSFET, a value of 1 or a logical high corresponded to the conduction state whereas a value of 0 or logical low corresponded to the off state as shown in Figure 3. The symbol ¬ indicates the NOT operator.

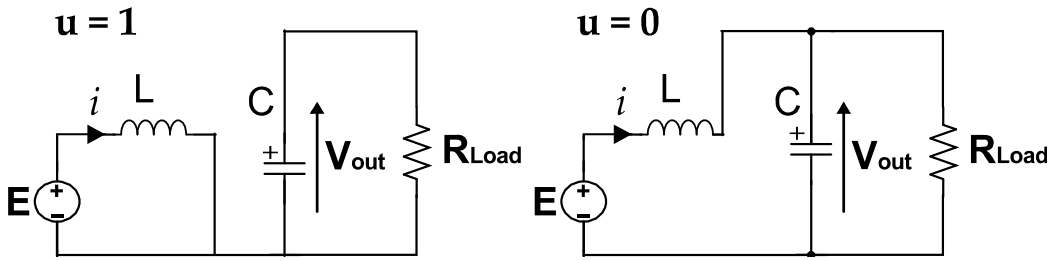


Figure 3. Boost converter conduction state for u = 1 and u = 0.

A state space model may be adopted to describes its behaviour in time where lowercase letter i denotes the input current to the converter, E, L and C are the input voltage, inductance and capacitor respectively.

$$\begin{bmatrix} \frac{di}{dt} \\ \frac{dV_{out}}{dt} \end{bmatrix} = \begin{bmatrix} 0 & -\frac{\neg u}{L} \\ \frac{\neg u}{C} & -\frac{1}{R_{load}C} \end{bmatrix} \begin{bmatrix} i \\ V_{out} \end{bmatrix} + \begin{bmatrix} \frac{E}{L} \\ 0 \end{bmatrix} \tag{5}$$

In order to operate the boost converter in current control mode an appropriate controller must be designed such that it would track a reference current, by applying the definition of the sliding surface S(x,t) [19]. For n = 1 and tracking erro $\tilde{x} = (i - i^{ref})$ i^{ref} being the desired current and i the measured current and λ a positive constant.

$$S(x,t) = (\frac{d}{dt} + \lambda)^{n-1} \tilde{x} = (\frac{d}{dt} + \lambda)^{0} (i - i^{ref}) \tag{6}$$

$$S = (i - i^{ref}) \tag{7}$$

A sliding surface S is recognized and for it to be valid, the control variable u must appear in the first derivative, we observe that is the case

$$\dot{S} = \frac{E}{L} - (\neg u)\frac{V_{out}}{L} - \frac{di^{ref}}{dt} \tag{8}$$

We assume that the current has high dynamic response and reach his desired value faster than we have Equation (9).

$$\begin{cases} i \to i^{ref} \\ \frac{di}{dt} \gg \frac{di^{ref}}{dt} \end{cases} \tag{9}$$

Thus, the reference signal may be omitted from the sliding surface derivative and a candidate Lyapunov's function is chosen for a stability analysis

$$B = \frac{1}{2}S^2 > 0 \tag{10}$$

The derivative of the Lyapunov function (10) becomes (11) as follows

$$\dot{B} = \dot{S}S = (\frac{E}{L} - (\neg u)\frac{V_{out}}{L})S < 0 \tag{11}$$

The gate driving signal u is a binary variable taking values of 0 or 1, since it's dependent on the surface it would be reasonable to apply the following Utkin control law [20]

$$\neg u = \frac{1}{2}sgn(S) + \frac{1}{2} \tag{12}$$

Checking the validity of the control law by applying the criterion and for a negative surface for $i^{ref} > i$

$$\dot{S}S = -|S|\frac{E}{L} < 0 \tag{13}$$

Since the voltage source E is considered a positive non null value the criterion is fulfilled for sgn(S)= -1. The same analogy is applied to the positive value of the surface

$$\dot{S}S = |S|\frac{E - V_{out}}{L} < 0 \tag{14}$$

The current control is stable so long $V_{out} > E$ (boost) and the reach time of the sliding surface is concluded

$$t_{reach} = \frac{|S_o|L}{E} \quad (\text{if } S < 0) \tag{15}$$

$$t_{reach} = \frac{|S_o|L}{(E - V_{out})} \quad (\text{if } S > 0) \tag{16}$$

Now that the stability of the system is proven, it would be logical to attempt finding out the transfer function that describes the sources current I_s dynamics in response to reference current I_s^{ref}. Starting from the trivial KVL and the subsequent relevant equations where the bar is used to denote the average value overtime, V_L inductance voltage, and δ average duty cycle.

$$V_L = \delta \cdot V_{out} - E \tag{17}$$

$$V_L = L\frac{di}{dt} \tag{18}$$

$$\delta = \neg\bar{u} \tag{19}$$

$$\frac{V_{out}}{V_{out}^{ref}} = \frac{1}{(R_{load}C \cdot s + 1)} \tag{20}$$

$$V_{out}^{ref} = R_{load}I_{laod} = R_{load} \cdot \delta \cdot i^{ref} \tag{21}$$

$$E = \delta \cdot V_{out} \tag{22}$$

$$I_s^{ref} = \delta \cdot i^{ref} \tag{23}$$

The model of current dynamic is acquired

$$\frac{I_s}{I_S^{ref}} = \frac{1}{(\frac{L}{\delta^2 R_{load}}s + 1)(R_{laod}C \cdot s + 1)} \tag{24}$$

From its canonical form the natural frequency and damping ratio are acquired

$$\frac{I_s}{I_S^{ref}} = \frac{\frac{\delta^2}{LC}}{s^2 + (\frac{\delta^2 R_{load}}{L} + \frac{1}{R_{laod}C})\cdot s + \frac{\delta^2}{LC}} \tag{25}$$

$$\omega_n = \frac{\delta}{\sqrt{LC}} \tag{26}$$

$$\zeta = \frac{\sqrt{LC}\cdot(\frac{\delta^2 R_{load}}{L} + \frac{1}{R_{load}C})}{2\delta} \tag{27}$$

2.1. Voltage Regulation

In order to ensure that the output voltage tracks its voltage reference a similar study is conducted coming from Equation (6) for n = 1 and $\widetilde{x} = (V_{out} - V_{out}^{ref})$,

$$S_2 = (V_{out} - V_{out}^{ref}) \tag{28}$$

$$\dot{S}_2 = \frac{1}{C}(I_S - I_{load}) - \dot{V}_{out}^{ref} + \Delta f(x) + \Delta d \tag{29}$$

This is a regulation problem where the input reference is a never changing constant value hence it's derivative could be omitted from the surface derivative equation, the terms $(\Delta f(x) + \Delta d)$ ertains to the system uncertainties arising from the non-linearity and losses of the system. Proceeding to conduct Lyapunov stability analysis

$$B_2 = \frac{1}{2}S_2^2 > 0 \tag{30}$$

$$\dot{B}_2 = \dot{S}_2 S_2 = (\frac{1}{C}(I_S - I_{load}) - \dot{V}_{out}^{ref} + \Delta f(x) + \Delta d)\cdot S_2 < 0 \tag{31}$$

In this case the control variable is the source's current as such one may include cancelling terms to simplify the control law. For the load current it's a measurable state hence can be compensated directly as for the terms $\Delta f(X)$ and Δd they are unknown, however, one approach to constructing a meaningful control law it to define boundaries β, α such that the aforementioned uncertainties may be contained within.

$$|(\Delta f(x)| \leq \alpha(x,t) \tag{32}$$

$$|\Delta d| \leq \beta(x,t) \tag{33}$$

The control law is chosen where K is an arbitrary control parameter.

$$I_s = I_{eq} + I_{comp} \tag{34}$$

$$I_{eq} = I_{load} \tag{35}$$

$$I_{comp} = (\alpha + \beta + K)\cdot sgn(S_2) \tag{36}$$

Proceeding to the stability analysis

$$\frac{1}{C}((\Delta f(x) + \alpha) + (\Delta d + \beta) + K)\cdot S_2 < 0 \quad (\text{if } S_2 < 0) \tag{37}$$

$$\frac{1}{C}((\Delta f(x) - \alpha) + (\Delta d - \beta) - K)\cdot S_2 < 0 \quad (\text{if } S_2 > 0) \tag{38}$$

The dual loop control scheme is displayed in Figure 4

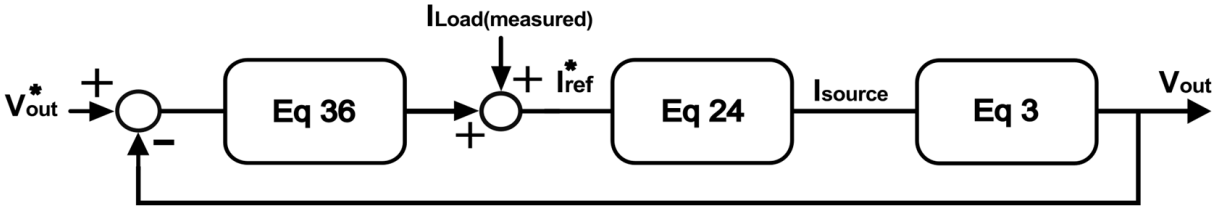


Figure 4. Global control loop for single source model. Where Equation (36) is the voltage controller, Equation (24) the transfer function (I_s/I_s^{ref}) and Equation (3) the transfer function (V_{out} /I_{source}).

2.2. Bi-Directional Current Flow

Utilizing a synchronous boost converter, illustrated in Figure 5, allows for the control of the current in both direction, this is particularly necessary when working with electrical energy storage that requires bi-directional capabilities for charging and discharging.

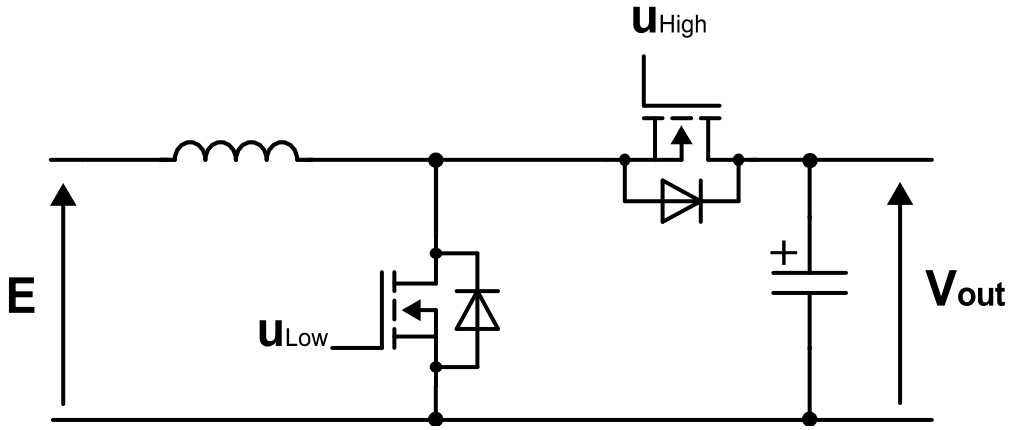


Figure 5. Synchronous bi-directional converter.

The gate signal on the high and low side are complimentary to one another, they can also be designed such that in boost mode, only the low side switch works and vice versa, in buck mode, only the high side switch is active [21].

It was shown that the reference current is the sum of the measured load current and the output of the voltage regulator (Equation (21)), when an arbitrary source participates in voltage regulation, a fraction of the current reference is passed to its controller. When the refence current has positive values the energy flows from the source to the load, hence the synchronous converter is in step-up or boost mode as shown in Figure 6. Conversely, when the reference value has negative values, in this case dictated by a batter charging manager block, the flow of energy reverses and the converter is set to step-down or buck mode illustrated in Figure 7. For applications like charging a battery, the battery side voltage must be precisely regulated. A charging battery can be modeled as a non-linear resistor, where its value depends on the integral of the current passing through it.

$$R_{bat} = f(\int_{t_o}^{t} I_{charging}(\tau)d\tau) \quad (39)$$

$$E^*_{charging} = R_{bat} I^*_{charging} \quad (40)$$

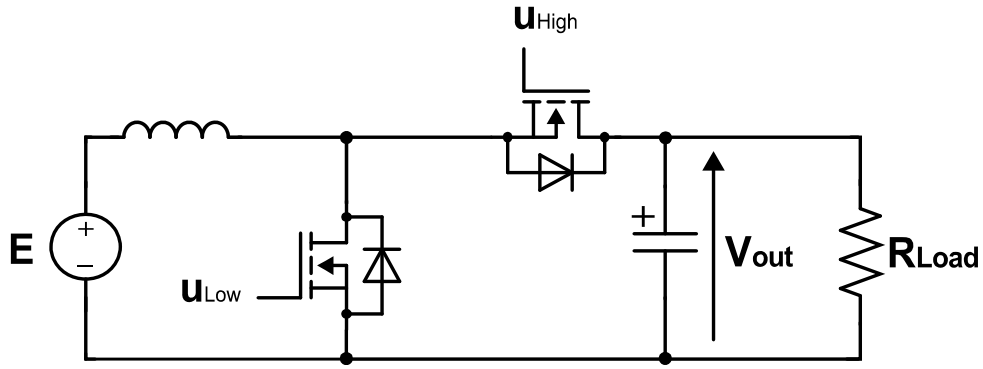


Figure 6. Synchronous converter in boost mode.

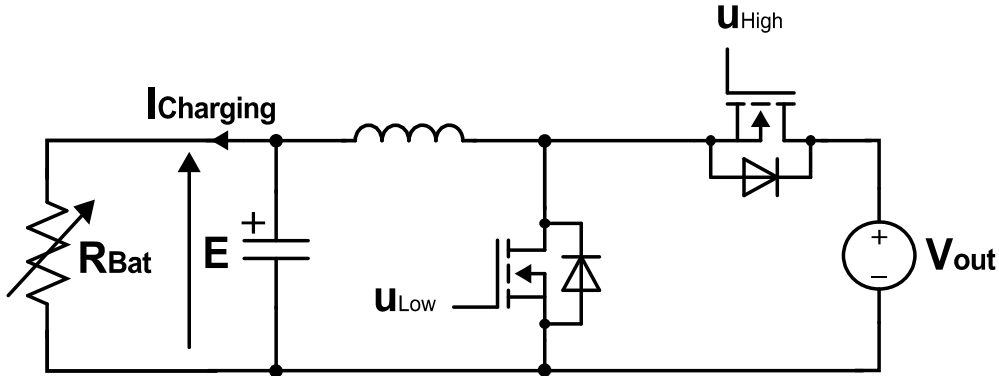


Figure 7. Synchronous converter in buck mode.

Equation (39) does not serve as a predictive model for battery behavior; rather, it simulates the change in load during charging. By utilizing historical data, an electronic load can emulate a battery if it is computer-controlled. For instance, a programmable load can be employed to replicate the charging process of a battery. This approach is frequently used in testing and development to simulate various battery conditions and behaviors without the need for an actual battery [22].

Starting from Equation (17) through (23) and adding the relevant Equations (41) through (47) pertaining to the transition between the buck and boost mode denoted "m" where δ_o is the threshold duty cycle for buck-boost operation mode and lowercase letter m the mode of operation.

$$E_s = \delta \cdot R_{load} I_{s-discharging} \tag{41}$$

$$V_{out} = (1-\delta)^{-2} \cdot R_{bat} I_{s-charging} \tag{42}$$

$$m = \frac{1}{2}\mathrm{sgn}(\delta - \delta_o) + \frac{1}{2} \tag{43}$$

$$\delta_o = 1 - \frac{E}{V_{out}} \tag{44}$$

$$I^*_{bat-char} = (1-\delta)^{-1} I_{s-char} \tag{45}$$

$$E_{bat} = \frac{R_{bat}(1-\delta)^{-1}}{(R_{bat}Cs+1)} I_{s-char} \tag{46}$$

$$I^*_s = mI^*_{s-dischar} + (\neg m)I^*_{s-dischar} \tag{47}$$

The complete buck-boost version of Equation (17)

$$V_L = m\delta V_{out(reg)} + (\neg m)E_{(reg)} - (\neg m)(1-\delta)V_{out-source} - mE_{source} \tag{48}$$

And the transfer function relating the reference current in the bi-directional flow of current

$$\frac{I_s}{I_S^{ref}} = \frac{\neg m}{(\frac{(1-\delta)L}{R_{bat}}s+1)(R_{bat}C{\cdot}s+1)} + \frac{m}{(\frac{L}{\delta^2 R_{load}}s+1)(R_{laod}C{\cdot}s+1)} \tag{49}$$

Continuing with the theme of this study, the hypothetical residential complex under analysis is modeled as parallel current-controlled sources (CCS) connected to a common bus according to the schematics in Figure 8. The primary sources involved in powering the load include solar panels, wind turbines, an electrical energy storage system (EESS or ESS), and a link converter (LCG) connected to the grid. These sources are the main producers of electrical energy. To enhance system reliability, backup sources such as ultra-capacitors, fuel cells, or diesel-powered generators may be included. The use of super-capacitors is particularly beneficial for stability, especially during transients, and can also provide short-term inertial response.

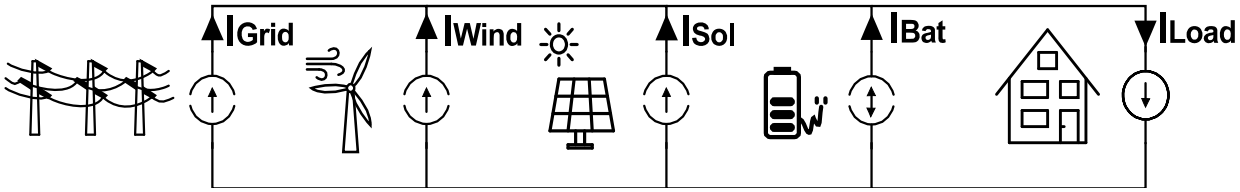


Figure 8. Microgrid multi current sources model.

Through the applications of the first and second laws of thermodynamics and knowing the total current entering a node is equal to that of the sum of currents departing from it, and noting that the voltage is regulated at a constant value, the linear combination

$$P_{in} - P_{loss} = [V_{out}][\theta][I_{sources}]^T = V_{out}I_{load} \tag{50}$$

where θ is the participation matrix contain values varying between 0 and 1, it also accounts for the efficiency of the converters. Each source contributes a percentage of the power to the system. The efficiency of the power electronics involved in high power application usually sits above 90% but as the power drops so do the yield, hence, an effective voltage regulation will require a robust control method to account for both uncertainties in the model and the nonlinearity of the efficiency. The schematics of the power electronics configuration is illustrated in Figure 9. This configuration is also referred to as a multi-input single output converter (MISO) [23].

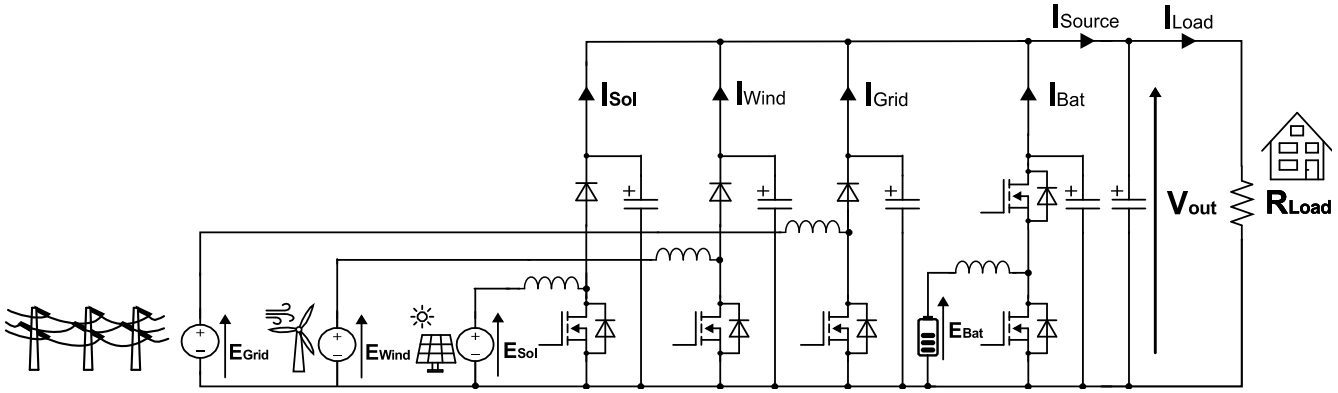


Figure 9. Microgrid multisource power electronics schematics.

As stated earlier, DC MGs offers an intuitive platform to conduct both a theoretical study and deploy experimental tests [24], since the voltage is regulated at a constant value,

all energy related analysis is done on the inner current control loop, in other words the problem of stability is decoupled from the problem of energy management which in turn can be formulated into an optimization problem. Figure 10, showcases the general structure of control; the output of the voltage regulation is considered an index of the energy required (denoted I^*_{ref}) to maintain the stability of the system.

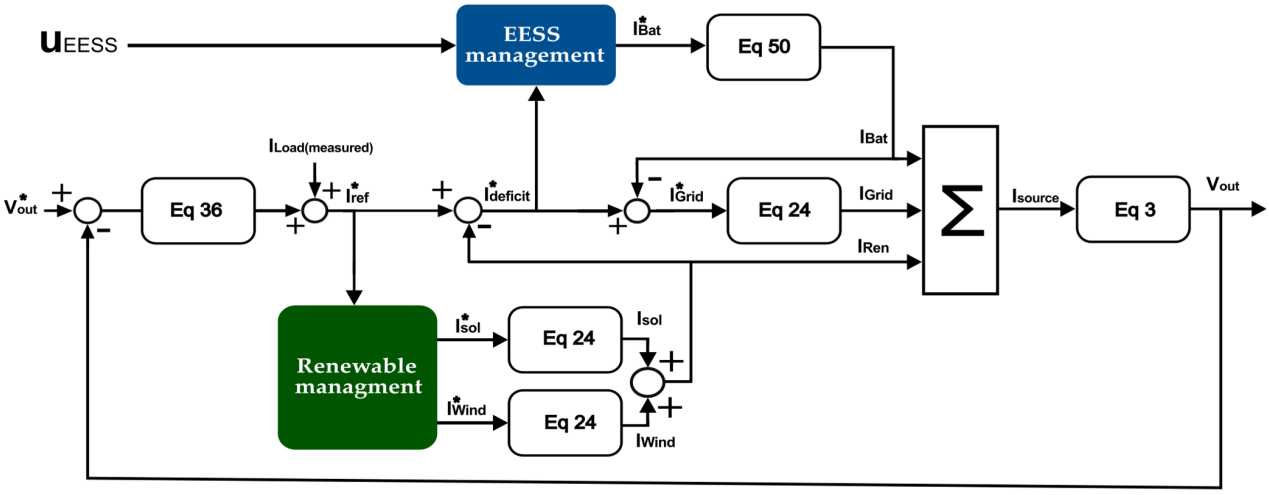


Figure 10. Control structure of the multi-source microgrid.

The index I^*_{ref} is used as a hard maximum limit for renewable energy management block in the production of energy with two modes of operations, Equations (51) and (52);

$$\text{if } (I^*_{ref} < I_{ren-max}) \quad \text{then } (I_{ren} = I^*_{ref}) \tag{51}$$

$$\text{if } (I^*_{ref} \geq I_{ren-max}) \quad \text{then } (I_{ren} = I_{ren-max}) \tag{52}$$

In the case where the renewables are able to supply 100% of the required energy the energy management block simply forwards the desired set point to the resources dispatching.

Else, when the required energy of the system exceeds that of the current renewable capacity, the maximum power point tracking (MPPT) algorithm is triggered, outputting the maximum current possible as disclosed in Figure 11.

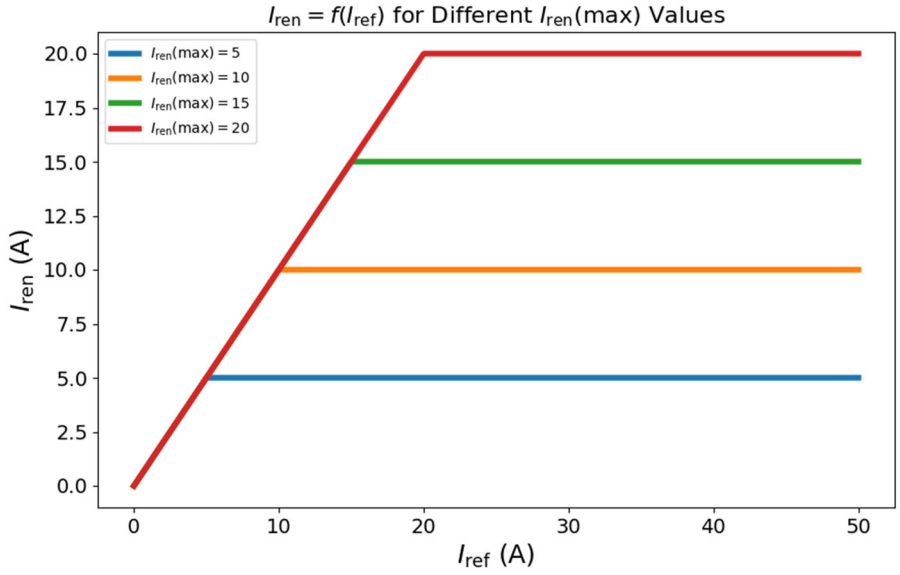


Figure 11. Output renewables current at different maximums.

In addition to enforcing strict system limits, the Energy Storage System (EESS) management block is responsible for overseeing protective mechanisms in the event of a fault. Moreover, depending on various scenarios, the EESS may be prompted to discharge and compensate for power imbalances. The storage capacity of the microgrid is directly correlated with the effectiveness of optimization methods, for this reason it is essential to manage the charging and discharging cycles properly. During the time of the day when energy is most inexpensive or free, the system initiates the charging process. In the subsequent provided illustration, a negative sign indicates charging, whereas a positive value indicates discharging. The state of charge (SOC) of the battery is maintained within an appropriate range to prevent premature degradation, Equation (53). Numerous other constraints can be specified, such as the number of charge/discharge cycles per day, the rate of consumption change, and voltage range.

$$\begin{cases} I_{char-rate} \leq I_{bat} \leq I_{dischar-rate} \\ 20\% \leq SOC \leq 80\% \\ (Cycles/day) < \text{allowable cycles times} \end{cases} \tag{53}$$

Demand side management (DSM) may also be employed as an additional energy management mechanism, by dividing the bus into two sperate lines one for critical loads and the another for non-critical loads, the DSM may then be able to reduce the total load in case of an emergency or with compliance to load shifting policies [25].

The inputs of the system can be intuitively divided into exogenous and actuators. The Renewable energy currents I^*_{sol} and I^*_{wind} are subject to constant unpredictable change, hence they can be thought of as disturbances to the system. I^*_{ref} is entirely dependent on the end-user and while it can be inferred or influenced, it cannot be determined therefore it is also considered a disturbance. U_{eess} is a deterministic value dependent on the preference of charging and discharging which can be preset to alter the system's outputs to desired values.

$$w = \begin{bmatrix} I^*_{ref} \\ I^*_{sol} \\ I^*_{wind} \end{bmatrix}, u = [u_{eess}] \tag{54}$$

The system then is rewritten into a representation of an optimization problem, the grid's current, z_1, is the variable to be optimized, whereas y_1, y_3 and y_3 are the measured states.

$$P = \begin{bmatrix} 1 & -T_1 & -T_2 & T_2 \\ 0 & T_3 & 0 & 0 \\ 0 & 0 & T_3 & 0 \\ 0 & 0 & 0 & T_3 \end{bmatrix} \begin{bmatrix} I^*_{ref} \\ ueess \\ I^*_{sol} \\ I^*_{wind} \end{bmatrix} = \begin{bmatrix} z_1 \\ y_1 \\ y_2 \\ y_3 \end{bmatrix} = \begin{bmatrix} I_{grid} \\ I_{bat} \\ I_{sol} \\ I_{wind} \end{bmatrix} \tag{55}$$

where: T_1 is the multiplication of Equation (50) and Equation (24), T_2 is the square of Equation (24) and T_3 is Equation (24).

3. Objectives

The significance of an effective Energy Management System (EMS) design on the MG cannot be overstated. It is a crucial component of the controller that ensures the optimization of system performance and electrical billing, while also facilitating the achievement of environmental sustainability goals. In this study, the MG is supposed to be controlled in such a way that it would fulfil an objective function that quantifies a multitude of economic and environmental interests [26]. Stability in the power system may refer to the ability of the MG to deliver quality electrical energy reliability in spite of any perturbation, naturally this goal takes priority especially in critical infrastructure. Stability is compromised when the grid deviates dangerously from its setpoint, potentially damaging the connected loads, or when it experiences a blackout. A load current that approaches the maximum capacity of the grid poses a threat to stability, hence, employing peak shaving and valley filling (PS

& VF) techniques [27], not only help with cost reduction but also assist tremendously with keeping healthy margins of stability. Additionally, in [28] a study was conducted showing the correlation between PS & VF and reduction of greenhouse gases (GHG) emissions. Of course, PS & VF has its limits depending on ESS characteristics and the flexibility of the end user. A work around this limitation can be achieved by adopting a region of inertial response, this limits the steepness of the grids current subsequently contributing to utility grid stability [29,30].

There are two means by which an effective management can be achieved. First are methods influencing the utility of end-user I^{*}_{ref}, through taxing or rewarding laws that would incentivize the end-user to modify the consumption behaviour, this is referred to as load shifting. A heavy-handed version of load shedding works by outright forcing the rotation of partial blackouts at peak hours between network districts in what is refer to as load shedding [31].

Other than load shedding and load shifting which are of great inconvenience to the end-user, EESS output power production is the only other control option for EMSs [32]. The task of energy management in practice can be also translated to flattening the curve of consumption. The task of flattening the curve not only is economically beneficial to the end-user, moreover it enhances the stability and alleviate the stress on the utility grid during peak demand hours. Ideally, a curve is flattened to its mean value, in practice that is seldom possible, however some insights can be determined from the concept. Figure 12 showcase an arbitrary consumption profile (CP) of a domicile [33].

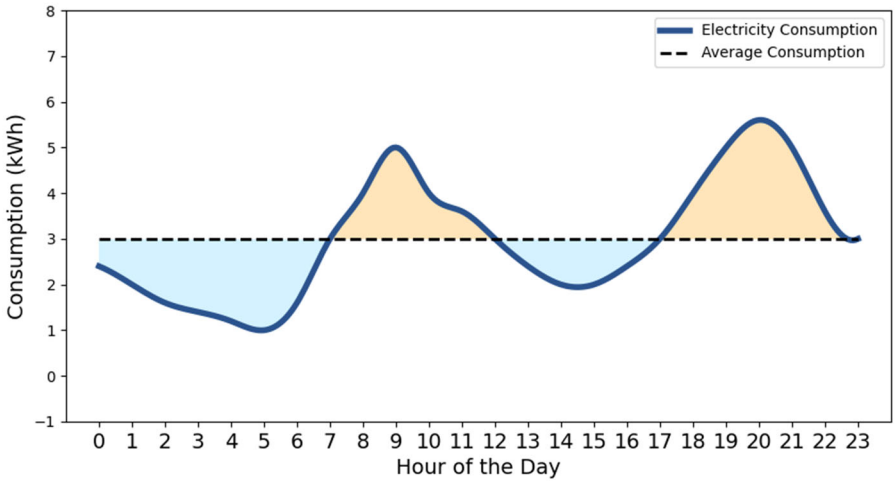


Figure 12. Typical daily electricity consumption profile of a domicile.

Ideally, the ESS should be able to charge when the load current is below average and discharge when the current is above the average, that will cause the load profile to turn into a flat line with no steep variation hence much easier to supply and regulate. In reality the ESS system has its own limitation. The fist hard limitation to be discussed is the capacity of storage, this constraint might cause the battery to suddenly disconnect in the middle of its expected operation. When SOC is below or over the allowed threshold, unexpected halt of ESS current can cause system instability; therefore, a mechanism of smooth disengaging from power production must be put in place. Another constraint adheres to the nominal charging and discharging current of the ESS, high crest factor of consumption profile indicates that the load current stary far away from the average line to an extent such that the ESS won't be able to adjust the current to the ideal average value, even with sufficient capacity, in other words and for all practical purposes; it is better to adopt a region of average power consumption rather than a fixed ideal average as illustrated in Figure 13. Average power consumption range is determined according to the capacity of the ESS and its nominal charging and discharging current. The ESS not only should strive to keep the CP between in the region but it also should counter react

any steep variation of the current inside the range. Peak shaving is more effective when targeting the uppermost area as energy prices spikes during high demand, whereas valley filling should consider the lowermost area when energy price is the lowest.

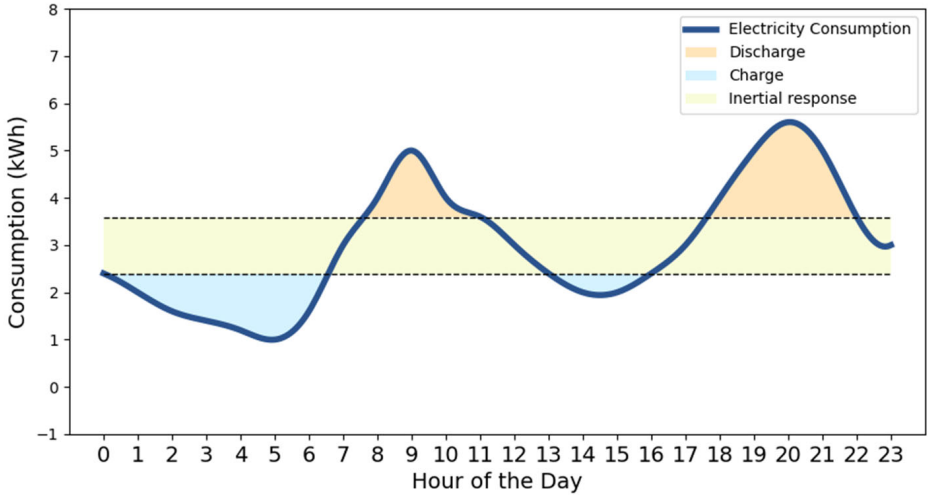


Figure 13. Modes of energy management.

Evidently, this plays a role in improving system stability by increasing the gap between the maximum power demand and the maximum capacity of the utility gird.

The CP of multi energy source MG (Figure 14) varies dependently on the availability of renewables, from previous discussions, prior knowledge of the average consumption value is a critical information on which the algorithm bases its decisions. Forecasting the consumption profile is a necessary procedure for decision synthesis, a multi variable utility function can be devised to that end taking into consideration the time of day, the day of week, reoccurring events, temperature, weather and many other variables [34]. Through accumulation of historical data and employment of advance machine learning it is possible to predict these parameters required for the optimization algorithm. Integrating renewables into the MG must take into consideration the dynamics of said sources. On the one side, introducing an energy source would most definitely reduce the electrical billing and improve overall reliability, however, abrupt untimely fluctuations in energy flow could elevate the stress on the utility power plants [35].

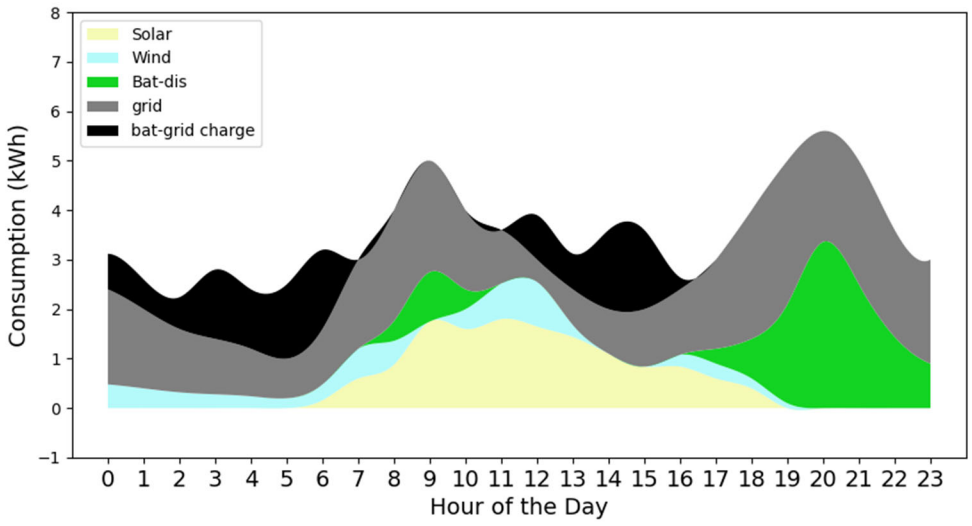


Figure 14. Simulated case of energy contribution in a multi-source microgrid.

The optimized controller is in fact a rule-based trading model that automates the functionality of the EESS, storing (buying) energy when it's cheapest then discharging later (selling) when it's most expensive. The performance of this model is evaluated every 24 h with indices that refers to the overall cost and the flatness of the consumption profile.

$$\begin{cases} C_{ost} = \beta_{price} \int_{t=0h}^{t=24h} I_{grid} e^{(r \cdot \beta_{flat})} dt \\ r = \left(\frac{I_{grid}}{I_{max}} \right)^{\beta_{stability}} - 1 \end{cases} \tag{56}$$

$$J_{flat} = \frac{T \cdot \beta_{price} \bar{I}_{grid} e^{(r \cdot \beta_{flat})}}{C_{ost}} \tag{57}$$

The economical cost is locally determined without the need for global communications as described in Equation (56), it is set such that it would increase exponentially as it approaches maximum energy production capacity. I_{max} denotes the maximum capacity of the bus and $\beta_{stability}$ the weight given for the penalty of approaching the maximum capacity, β_{flat} scales the exponential curves to highlight the contrast between low consumption and high consumption, whereas β_{price} is a linear coefficient that can either be set to a static value or be communicated with the provider. These coefficients shape the objective function towards the user preferences. The exponential penalizing of the grid's current doesn't just encompass the economical objective but it also extends to the green objective, less use of the utility gird means less GHG emissions. The variable "r" is the normalized index of stable operation, in Equation (7), when the surface was selected, it was assumed that the source is able to provide an infinite supply of energy, however, in reality the system is bounded by a power rating. For positive values of "r" the system stability is compromised. Equation (57) denotes the evaluation of energy management performance; the numerator is the economic cost calculated at $\bar{I}_{grid}$, which is the average consumption of current from the grid. The denominator on the other hand is the previously calculated economical cost of the MG, the evaluation is performed every period T. As a result of the exponential nature of the economic cost function, any late valley filling or premature peak shaving is penalized when contrasted against the calculated cost at perfectly flat average current.

4. Simulation

The simulation recreates the set up in Figure 9 subject to the control structure in Figure 10 where the all the sources are current controlled. The sources have different voltage levels varying with time, a common frame of study must be adopted. This is easy to accomplish since the currents at converters' output are proportional to those at input with a gain that depends on the ratio of source's voltage to bus voltage multiplied by a yield factor η. It may prove difficult to estimate the efficiency factor η however by employing adaptive control and robust methods this difficulty can be mitigated. Finally, by applying the previously conceptualized general control structure in Figure 10, it is possible to arrive at eight main bodies of control. First the "Voltage regulator and production routing", as the name suggest this block contain the voltage regulator used in the simulation, its outputs with conjunction with the feedback from dispatching units handles and coordinates the assignment of energy dispatching required for voltage stability. The estimator and MPPT block responsible for maximizing renewables' output power when necessary. The EESS battery manager system (BMS), is the body of control responsible for producing the current set point of the battery. Moreover, it imposes the hard limits of the SOC as well as charging cycles in the interest of extending ESS longevity. Demand side management block is responsible for load shifting in correspondence to incentivizing laws, in case of a fault or an emergency the DSM perform load shedding to retains the stability of the system. In addition, there are three dispatching unites for renewables, battery and grid power electronics that ensures that the set point is in effect. Finally, the EMS, monitors and manage the whole ensemble of the system, it performs background tasks such as

data collection, parameters inferring, anomaly detection and most importantly it runs the decision-making algorithms responsible for attaining the objective function.

Results

The simulated CP alongside renewables profile and battery current of the multi-source MG can be observed in Figure 15. In this iteration the valley filling current is set to 0.1 pu while peak shaving is set to 0.5 pu. The negative values of purple line representing the current of the ESS signifies the charging whereas positive values are for discharging. It could be seen that the charging starts after mid night mostly from wind energy and stops around 7 a.m., while discharging start at 3 p.m. and ends at 7:30 p.m.

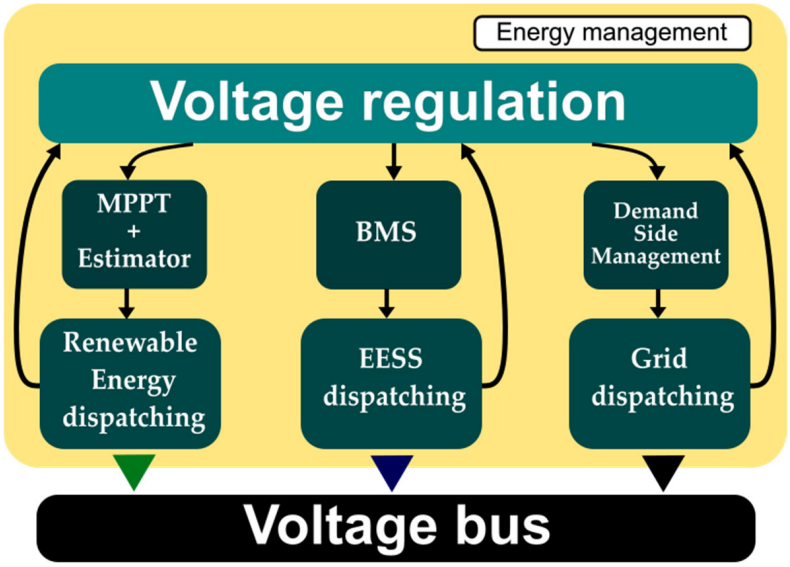


Figure 15. General diagram of the simulation.

Figure 16 discloses the evolution of the bus's voltage in time with a reference voltage of 60 V. Even though there are multiple sources participating in power production (Figure 17) at fluctuating rates, the voltage maintains its stability and does not deviate beyond tolerance. That being said, this structure of control is highly dependent on communications between the sources and the central command block which is a major drawback [36].

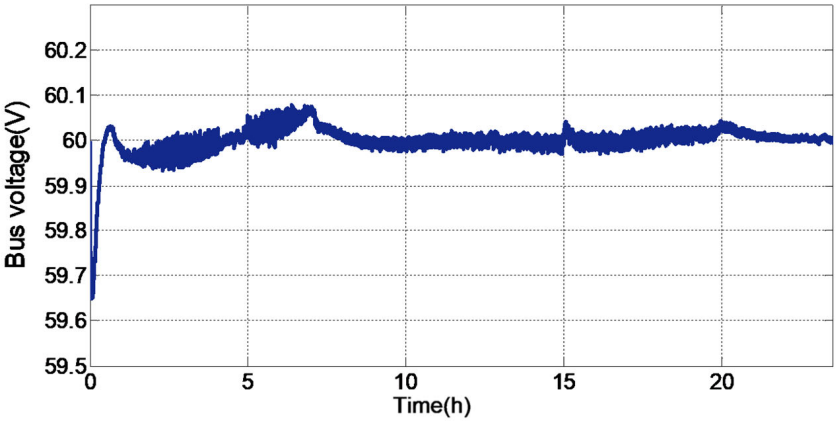


Figure 16. MATLAB SIMULINK simulated output voltage of a multi-source MG.

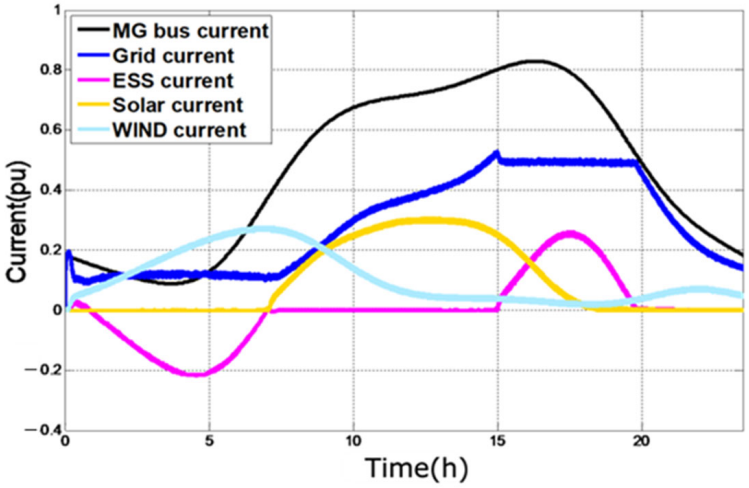


Figure 17. MATLAB SIMULINK simulation CP and sources contributions.

The voltage and SOC of the battery are shown in Figure 18, the curves are quite typical showing the expected increase and decrease in both voltage and SOC following charging and discharging. It is noteworthy that the initial SOC in quite close to its final value which could be taken as an indicator of good performance.

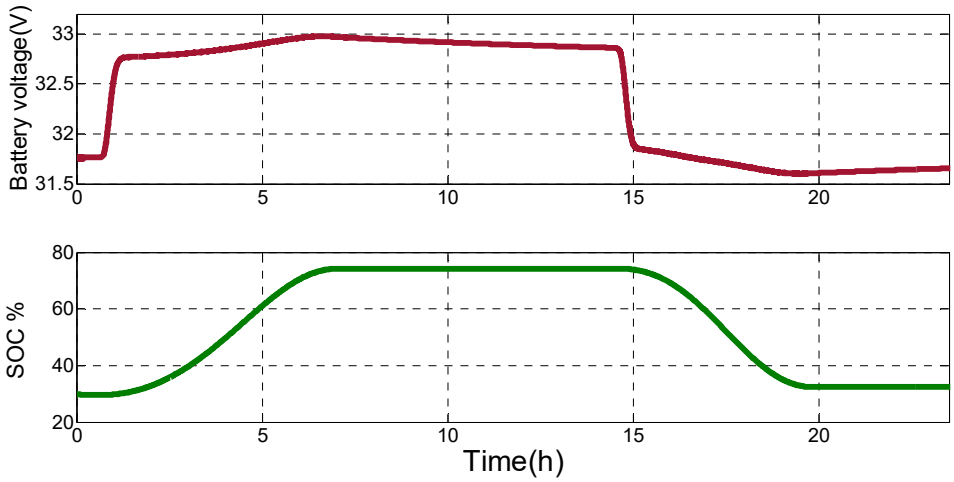


Figure 18. MATLAB SIMULINK simulation voltage and SOC of a battery.

Table 1 showcases the cost function correlation with the choice of VF&PS currents and the resulting local cost. The currents I_{VF} and I_{PS} are normalized to I_{max} the maximum current of the bus, the local cost is normalized to cost of an absolute flat CP, similarly a value of 1 for J flat index represent a completely flat line. Although the total amount of energy stays practically the same (not considering losses in the ESS), the local cost index decreases as the curve approaches resembling a flat profile. The data collected is fed to a machine learning process in order to enhance system performance, as well as building a forecasting model to keep the end-user well informed about the consumption patterns expected. For the effective analysis of these latter different time scales must be adopted (Daily, weekly, monthly and seasonal).

Another critical factor that must be taken into consideration is the rate of change of the CP. A fast change in load current puts strain on utility grid as production ramping takes place. An inertial response to abrupt or steep variation in load's current gives the utility grid enough time to respond properly and keep both quality and stability up to norms. In the case of the work conducted in this paper, an inertial factor denoted K is used to determine the supply of energy in proportion to variation. In Figure 19, At time t = 9:00 am, a surge of load current

is simulated and the counterreaction of the ESS is recorded. For K =1000 no reaction is observed from the ESS on the contrary for K = 2, the ESS largely mitigates the effect of the load surge.

Table 1. Local cost function correlation to the choice of charging and discharging battery currents.

I_{VF} (pu)	I_{PS} (pu)	Local Cost (pu)	J Flat (pu)
0	0.8	12.8457	0.2526
0.05	0.68	11.9649	0.2955
0.08	0.6	9.6683	0.3356
0.15	0.5	6.8976	0.5126
0.2	0.4	4.6929	0.7534

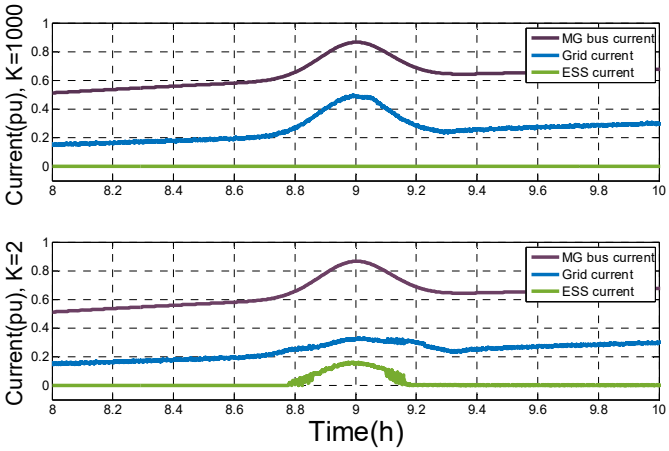


Figure 19. MATLAB SIMULINK simulation inertial response for K = 2 and K = 1000.

The proper management of inertial response is paramount, and unnecessary depletion or Repletion effect negatively the performance and operation of VF&PS. Supercapacitors can help immensely during inertial response due to their high discharge current burst capabilities. This in turn assures the longevity of the ESS.

5. Experimental Results

To ensure proper manipulation, it was first necessary to test and calibrate the feedback sensors connected to the R&D board's ADCs and its PWM channels controlling the power switches involved. Current control was tested, where all the different sources were able to participate successfully in supply power to the DC bus. A programmable load was configured in CV mode to absorb current and prevent overvoltage on the DC bus. The software used simulated the consumption profile and availability of renewable energies producing appropriate set points for the corresponding power converters.

The experiment conducted seeks to emulate as many real physical parts as possible, in cases where physical parts were unavailable, an integrated software component was used as a substitute. In this particular example, the setup (in Figure 20) is made of five main parts; the main group of hardware consist of (1) the current controlled 30 V, 3 A voltage sources representing the LCG, battery (discharge mode), wind driven power plant and solar panel. (2) The programmable load (PL) AEL-5000 is used as a dummy load to emulate the consumer demand. While it is possible to control the current going to the PL via an Ethernet medium, instead it is set in constant voltage (CV) mode, then it is connected to the bus via a boost converter according to the schematics in Figure 21 subsequently resulting in faster run time. (3) and (4) current controlled DC-DC converters. (5) computational system for the implementation of the software part, the availability of renewables is inferred in a predetermined in the software used as lookup tables; this provides a necessary degree of freedom in order to direct the experiment more efficiently and in a timely manner. The

battery response is emulated thanks to the combination of software model that output reference points in real-time and hardware consisting of for CCS for discharging and buck in conjunction with a resistor for charging.

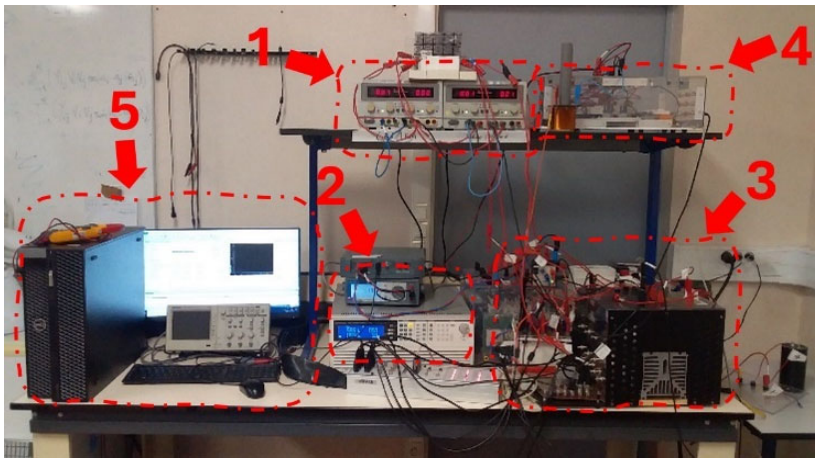


Figure 20. Test bed laboratory set up.

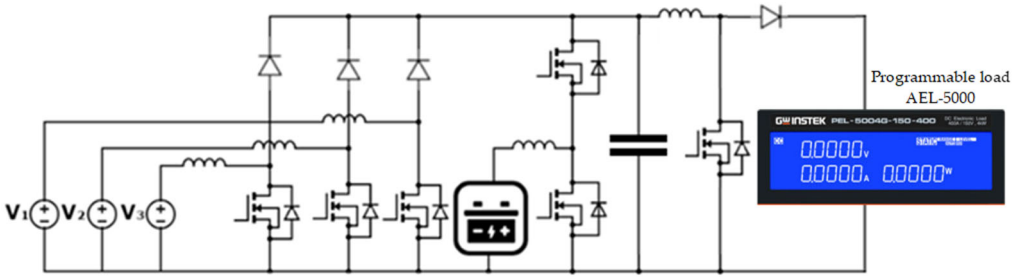


Figure 21. Experimental schematics of the MG.

The CV mode parameter is set to 75 V, while the bus voltage is regulated at 60 V, hence ensuring that the PL does not participate in voltage regulation. Finally, the dSPACE DS1104 R&D Controller Board, where all the developed controller, system models, look up table and algorithm are deployed in accordance with the previously review theoretical content.

Figures 22 and 23 display the evolution of the bus's voltage in time, as it can be observed the controller retains the voltage in its tolerance zone indicating the suitability of the control scheme used for this application.

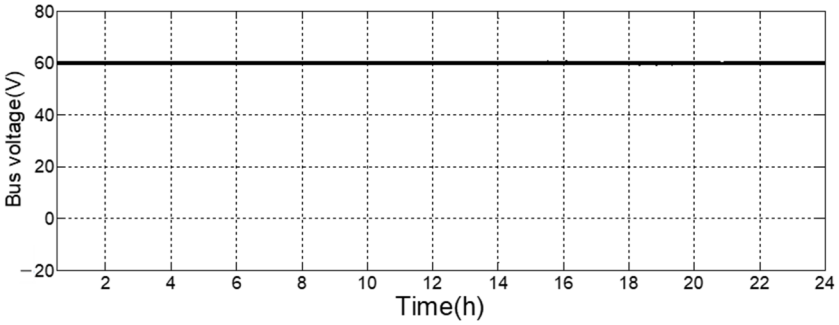


Figure 22. Experimental results of MG's bus voltage.

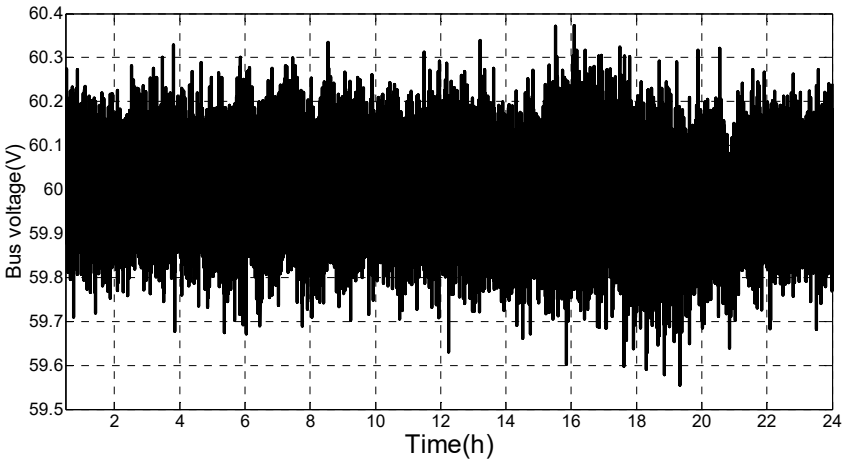


Figure 23. Zoomed in view of the Experimental results of MG's bus voltage.

Figure 24 could be considered the highlights of this paper's work, the experimental results disclosed are similar to those in the simulation because variables such as wind and solar availability as well as the CP are recorded in lookup tables and then inserted as set point in time for the current controlled sources and bus.

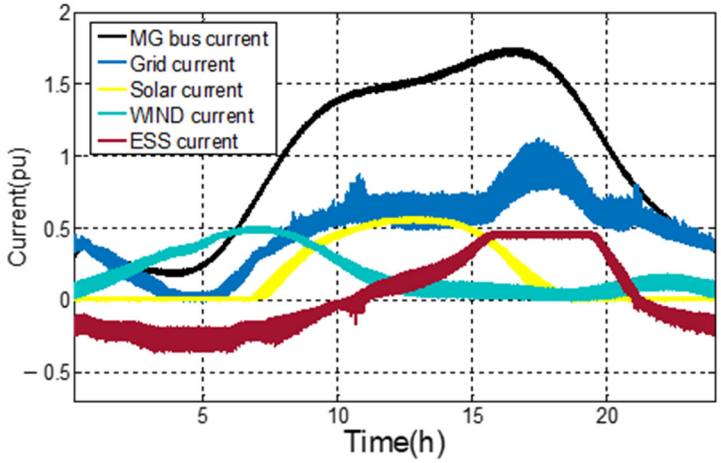


Figure 24. Emulated multi energy source MG CP.

It is entirely feasible to replicate the currents observed in the simulation within an experimental setup. The consumption profile current, solar panel current, and wind generation current are elements of the experiment itself, from the simulation, data has been stored in a lookup table in MATLAB SIMULINK then subsequently used as set points for current control of the ensemble (DC source + DC-DC converter), resulting in identical appearances. The discrepancy between the simulation and experimental can be observed in the battery current, the instrumental ensemble that emulated the battery had different characteristic to that of the simulation, the profile of the charging was sub-optimal yet it diffidently improved the whole grid performance, subsequently this effected the grid current which should not be confused with the load current (consumption profile).

The charging curve exhibits a non-uniform profile, particularly during the time interval from 15:30 to 17:30, where a noticeable hump is observed. This anomaly arises as the system reaches the nominal discharging current, indicating the termination of control extension. During this period, the only viable method to achieve a flattened curve is through load shedding.

6. Conclusions

This paper presents a comprehensive analysis of the regulation and management of a multi-source microgrid from an energy perspective. The study developed a versatile model applicable to both the analysis and design of microgrids. Additionally, the paper included detailed reports on the theoretical and experimental materials used to establish a control structure for an emulated microgrid, aimed at implementing an optimized energy management system. The deployment of such a system in urban areas is advocated due to its economic benefits and ecological advantages. Central to this experiment is the electrical storage system, whose efficient utilization is crucial for flattening the CP curve. This system is, in fact, the most convenient and versatile tool for energy management.

The experiment successfully conducted a simultaneous analysis of stability and energy, elucidating the relationship between the two. This dual focus is a distinctive feature not commonly observed in many other testbeds.

For further improvements on this subject, research should prioritize the development of a socio-economic model capable of accurately predicting the consumption load profile. This model should incorporate advanced data analytics, machine learning techniques to enhance and AI.

Author Contributions: Conceptualization, M.-D.D., S.H., A.N.-S., S.D. and L.C.-A. and S.L.; methodology, S.D.; software, M.-D.D. and S.D.; validation, M.-D.D., S.D., L.C.-A. and A.N.-S.; formal analysis, S.D. and L.C.-A.; investigation, M.-D.D. and S.D.; resources, M.-D.D.; data curation, S.D.; writing—original draft preparation, M.-D.D.; writing—review and editing, M.-D.D., S.H., A.N.-S., S.D. and L.C.-A.; visualization, S.D., S.L. and L.C.-A.; supervision, S.H., A.N.-S. and S.D.; project administration, S.H., A.N.-S. and S.D.; funding acquisition, Not Available. All authors have read and agreed to the published version of the manuscript.

Funding: This research received no external funding.

Institutional Review Board Statement: Not applicable.

Informed Consent Statement: Not applicable.

Data Availability Statement: Data are contained within the article.

Conflicts of Interest: The authors declare no conflict of interest.

Nomenclature

The following abbreviations are used in this manuscript:

$I_{sources}$	Converter output current, (Source current)
I_{load}	Load's current
i	Converter input current.
I_{ren}	Renewable current
I_{sol}	Current of the photovoltaic system (solar)
I_{wind}	Current of the wind power system.
$\beta_{stability}$	Penalty weight for approaching the maximum capacity
β_{flat}	Contrast weight
β_{price}	Linear energy price
C_{ost}	Cost
I_{ref}	Reference current
V_{out}	Output voltage
$V_{out\text{-}source}$	Output voltage in battery charging mode
$V_{out\text{-}reg}$	Output voltage in battery discharging mode
V_L	Inductance voltage of the simple boost converter
$I_{grid,}$ $\bar{I}_{grid}$	Current drawn from the grid and its average value.
r	normalized index of stable operation
I_{bat}	Battery current
$I_{s\text{-}char}$	Source charge current
$I_{s\text{-}dischar}$	Source discharge current

R_{bat}	equivalent battery resistor
T	Evaluation period
MPPT	Maximum power point tracking
PWM	Pulse width modulation
EESS	Electrical Energy storage system (or ESS)
SOC	State of charge
MG	Micro-grid
DC	Direct current
ζ	Damping coefficient
ω_n	Natural frequency
δ, δ_o	Duty cycle of the system and threshold duty cycle for buck-boost operation mode
β, α	Bounding control parameters
m	Mode of operation
θ	Contribution matrix
u_{eess}	Energy storage system control variable
CP	Consumption profile
CCS	Current controlled sources
KVL	Kirchhoff's voltage law
LCG	Link converter connected to the grid
PS & VF	Peak shaving and valley filling
GHG	Greenhouse gases
DSM	Demand side management
EMS	Energy management system
MISO	Multi-Input Single Output converter

References

1. Satapathy, A.S.; Mohanty, S.; Mohanty, A.; Rajamony, R.K.; Soudagar, M.E.M.; Khan, T.M.Y.; Kalam, M.A.; Alij, M.M.; Bashir, M.N. Emerging Technologies, Opportunities and Challenges for Microgrid Stability and Control. *Energy Rep.* **2024**, *11*, 3562–3580. [CrossRef]
2. Sarvi, M.; Zohdi, H.Z. A Comprehensive Overview of DC-DC Converters Control Methods and Topologies in DC Microgrids. *Energy Sci. Eng.* **2024**, *12*, 2017–2036. [CrossRef]
3. Naseri, N.; Aboudrar, I.; El Hani, S.; Ait-Ahmed, N.; Motahhir, S.; Machmoum, M. Energy Transition and Resilient Control for Enhancing Power Availability in Microgrids Based on North African Countries: A Review. *Appl. Sci.* **2024**, *14*, 6121. [CrossRef]
4. Ton, D.T.; Smith, M.A. The U.S. Department of Energy's Microgrid Initiative. *Energies* **2012**, *5*, 2021–2034. [CrossRef]
5. Lasseter, R.H.; Paigi, P. Microgrid: A Conceptual Solution. In Proceedings of the 2004 IEEE 35th Annual Power Electronics Specialists Conference (IEEE Cat. No. 04CH37551), Aachen, Germany, 20–25 June 2004; IEEE: New York, NY, USA, 2004.
6. Chrifi-Alaoui, L.; Drid, S.; Ouriagli, M.; Mehdi, D. Overview of Photovoltaic and Wind Electrical Power Hybrid Systems. *Energies* **2023**, *16*, 4778. [CrossRef]
7. Ahmad, S.; Shafiullah, M.; Ahmed, C.B.; Alowaifeer, M. A Review of Microgrid Energy Management and Control Strategies. *IEEE Access* **2023**, *11*, 21729–21757. [CrossRef]
8. García Vera, Y.E.; Dufo-López, R.; Bernal-Agustín, J.L. Energy Management in Microgrids with Renewable Energy Sources: A Literature Review. *Appl. Sci.* **2019**, *9*, 3854. [CrossRef]
9. Arévalo, P.; Ochoa-Correa, D.; Villa-Ávila, E. Optimizing Microgrid Operation: Integration of Emerging Technologies and Artificial Intelligence for Energy Efficiency. *Electronics* **2024**, *13*, 3754. [CrossRef]
10. Ali, S.; Zheng, Z.; Aillerie, M.; Sawicki, J.-P.; Péra, M.-C.; Hissel, D. A Review of DC Microgrid Energy Management Systems Dedicated to Residential Applications. *Energies* **2021**, *14*, 4308. [CrossRef]
11. Elazab, R.; Abo Dahab, A.; Abo Adma, M.; Hassan, H.A. Reviewing the Frontier: Modeling and Energy Management Strategies for Sustainable 100% Renewable Microgrids. *Appl. Sci.* **2024**, *6*, 168. [CrossRef]
12. Zahraoui, Y.; Alhamrouni, I.; Mekhilef, S.; Basir Khan, M.R.; Seyedmahmoudian, M.; Stojcevski, A.; Horan, B. Energy Management System in Microgrids: A Comprehensive Review. *Sustainability* **2021**, *13*, 10492. [CrossRef]
13. Liu, X.-K.; Wang, Y.-W.; Lin, P.; Wang, P. Distributed Supervisory Secondary Control for a DC Microgrid. *IEEE Trans. Energy Convers.* **2020**, *35*, 1736–1746. [CrossRef]
14. Ullah, M.H.; Babaiahgari, B.; Alseyat, A.; Park, J.-D. A Computationally Efficient Consensus-Based Multiagent Distributed EMS for DC Microgrids. *IEEE Trans. Ind. Electron.* **2021**, *68*, 5425–5435. [CrossRef]
15. Habibullah, A.F.; Kim, K.-H. Decentralized Power Management of DC Microgrid Based on Adaptive Droop Control with Constant Voltage Regulation. *IEEE Access* **2022**, *10*, 129490–129504. [CrossRef]
16. Padilla-Medina, A.; Perez-Pinal, F.; Jimenez-Garibay, A.; Vazquez-Lopez, A.; Martinez-Nolasco, J. Design and Implementation of an Energy-Management System for a Grid-Connected Residential DC Microgrid. *Energies* **2020**, *13*, 4074. [CrossRef]

17. Hwang, H.; Lee, S.H.; Choi, D.; Choi, S.; Sung, B. Voltage Stability Assessment of a Campus DC Microgrid Implemented in Korea as a Blockchain-Based Power Transaction Testbed. *Energies* **2023**, *16*, 7297. [CrossRef]
18. Mechnane, F.; Drid, S.; Nait-Said, N.; Chrifi-Alaoui, L. Robust Current Control of a Small-Scale Wind–Photovoltaic Hybrid System Based on the Multiport DC Converter. *Appl. Sci.* **2023**, *13*, 7047. [CrossRef]
19. Li, W.; Slotine, J.-J.E. *Applied Nonlinear Control*; Prentice-Hall, Inc.: Upper Saddle River, NJ, USA, 1990; pp. 276–307.
20. Guldner, J.; Shi, J.; Utkin, V. *Sliding Mode Control in Electro-Mechanical Systems*; Taylor & Francis: London, UK, 1999; p. 232.
21. Bhardwaj, M. *Modeling Bi-Directional Buck/Boost Converter for Digital Control Using C2000 Microcontrollers*; Application Report SPRABX5; Texas Instruments Incorporated: Dallas, TX, USA, 2015; p. 11.
22. Vergori, E.; Mocera, F.; Somà, A. Battery Modelling and Simulation Using a Programmable Testing Equipment. *Computers* **2018**, *7*, 20. [CrossRef]
23. Sun, Z.; Bae, S. Multiple-Input Soft-Switching DC–DC Converter to Connect Renewable Energy Sources in a DC Microgrid. *IEEE Access* **2022**, *10*, 128380–128391. [CrossRef]
24. Gao, F.; Kang, R.; Cao, J.; Yang, T. Primary and secondary control in DC microgrids: A review. *J. Mod. Power Syst. Clean Energy* **2019**, *7*, 227–242. [CrossRef]
25. Bakare, M.S.; Abdulkarim, A.; Zeeshan, M.; Shuaibu, A.N. A Comprehensive Overview on Demand Side Energy Management Towards Smart Grids: Challenges, Solutions, and Future Directions. *Energy Inform.* **2023**, *6*, 262. [CrossRef]
26. Vivas, F.J.; Segura, F.; Andújar, J.M.; Palacio, A.; Saenz, J.L.; Isorna, F.; López, E. Multi-Objective Fuzzy Logic-Based Energy Management System for Microgrids with Battery and Hydrogen Energy Storage System. *Electronics* **2020**, *9*, 1074. [CrossRef]
27. Chua, K.H.; Bong, H.L.; Lim, Y.S.; Wong, J.; Wang, L. The State-of-the-Arts of Peak Shaving Technologies: A Review. In Proceedings of the 2020 International Conference on Smart Grid and Clean Energy Technologies (ICSGCE), Kuching, Malaysia, 4–7 October 2020; pp. 162–166.
28. Zhang, L.; Yang, Y.; Li, Q.; Gao, W.; Qian, F.; Song, L. Economic optimization of microgrids based on peak shaving and CO2 reduction effect: A case study in Japan. *J. Clean. Prod.* **2021**, *321*, 128973. [CrossRef]
29. Brinkel, N.B.G.; Gerritsma, M.K.; AlSkaif, T.A.; Lampropoulos, I.; van Voorden, A.M.; Fidder, H.A.; van Sark, W.G.J.H.M. Impact of rapid PV fluctuations on power quality in the low-voltage grid and mitigation strategies using electric vehicles. *Int. J. Electr. Power Energy Syst.* **2020**, *118*, 105741. [CrossRef]
30. Eriksson, R.; Modig, N.; Elkington, K. Synthetic inertia versus fast frequency response: A definition. *IET Renew. Power Gener.* **2018**, *12*, 507–514. [CrossRef]
31. Amasyali, K.; Chen, Y.; Telsang, B.; Olama, M.; Djouadi, S.M. Hierarchical Model-Free Transactional Control of Building Loads to Support Grid Services. *IEEE Access* **2020**, *8*, 219367–219377. [CrossRef]
32. Linden, D.; Reddy, T.B. *Handbook of Batteries*, 3rd ed.; McGraw-Hill: New York, NY, USA, 2001.
33. Proedrou, E. A Comprehensive Review of Residential Electricity Load Profile Models. *IEEE Access* **2021**, *9*, 12114–12133. [CrossRef]
34. Nakajima, K.; Takane, Y.; Fukuba, S.; Yamaguchi, K.; Kikegawa, Y. Urban electricity temperature relationships in the Tokyo Metropolitan Area. *Energy Build.* **2022**, *256*, 111729. [CrossRef]
35. Cai, H.; Shen, S.; Lin, Q.; Li, X.; Xiao, H. Predicting the Energy Consumption of Residential Buildings for Regional Electricity Supply-Side and Demand-Side Management. *IEEE Access* **2019**, *7*, 30386–30397. [CrossRef]
36. Muyizere, D.; Letting, L.K.; Munyazikwiye, B.B. Effects of Communication Signal Delay on the Power Grid: A Review. *Electronics* **2022**, *11*, 874. [CrossRef]

Disclaimer/Publisher's Note: The statements, opinions and data contained in all publications are solely those of the individual author(s) and contributor(s) and not of MDPI and/or the editor(s). MDPI and/or the editor(s) disclaim responsibility for any injury to people or property resulting from any ideas, methods, instructions or products referred to in the content.